# Individual wave overtopping volumes on mound breakwaters in breaking wave conditions and gentle sea bottoms

Patricia Mares-Nasarre [1, *], Jorge Molines[1], M. Esther Gómez-Martín[1] and Josep R. Medina[1]

[1] Lab. Ports and Coasts, Institute of Transport and Territory, Universitat Politècnica de València; patmana@cam.upv.es, jormollo@upv.es, mgomar00@upv.es, jrmedina@upv.es.

* Corresponding author: patmana@cam.upv.es

**Abstract:**

Mound breakwaters are usually designed to limit the mean wave overtopping rate ($q$) or the maximum individual wave overtopping volume ($V_{max}$). However, rarely do studies focus on wave overtopping volumes on breakwaters in depth-limited breaking wave conditions. This study analyzes 2D physical tests on mound breakwaters with relevant overtopping rates ($0.33 \leq R_c/H_{m0} \leq 2.83$) and three armor layers (Cubipod®-1L, rock-2L and cube-2L) in depth-limited breaking wave conditions ($0.20 \leq H_{m0}/h_s \leq 0.90$) and with two bottom slopes ($m$ = 1/25 and $m$ = 1/50). The 2-parameter Weibull distribution was used to estimate $V_{max}^* = V_{max}/(g\, H_{m0}\, T_{01}^2)$ with coefficient of determination $R^2$ = 83.3%. In this study, the bottom slope ($m$ = 1/50 and $m$ = 1/25) did not significantly influence $V_{max}$ or the number of overtopping events, $N_{ow}$. During the design phase of a mound breakwater, $q$ is required to use the methods given in the literature to estimate $V_{max}$. Thus, $q$ must be estimated for design purposes when measured $q$ is not available. In this study, CLASH Neural Network (CLASH NN) was used to estimate $q$ with $R^2$ = 63.6%. If the 2-parameter Weibull distribution proposed in this study is used to estimate $V_{max}$ with $q$ estimated using CLASH NN, the prediction error of $V_{max}^*$ is $R^2$ = 61.7%. With the method presented in this study, the ratio between estimated and measured $V_{max}^*$ falls within the range 1/2 to 2 (90% error band) when $q$ is estimated with CLASH NN. The new estimators derived in this study provide good predictions of $N_{ow}$ and $V_{max}$ with a method simpler than those in the literature on overtopped mound breakwaters in depth-limited breaking wave conditions on gentle sea bottoms ($1/50 \leq m \leq 1/25$).

**Keywords:** mound breakwater; wave overtopping; individual wave overtopping volumes; depth-limited breaking wave conditions; bottom slope; proportion of overtopping events

## 1. Introduction

Crest elevation is a key parameter when designing mound breakwaters due to its direct effect on construction costs as well as visual and environmental impact. Climate change effects (e.g., sea level rise) and increasing social concern about the visual impact of coastal structures are leading to reductions in crest freeboards and increases in the overtopping hazard. In this situation, coastal structure designs with reduced crest freeboards and relevant overtopping discharges become significant. In addition, most mound breakwaters are built in the surf zone, where they are attacked by waves breaking on the sea bottom.

Tolerable mean overtopping discharges, $q$ (m³/s/m), are commonly considered to design crest elevation of coastal structures. However, the mean individual overtopping volume ($\bar{V}$) may be much lower than the maximum individual wave overtopping volume, $V_{max}$ (m³/m). For this reason, Franco et al. (1994) suggested that overtopping hazard should be directly related with individual wave overtopping events, rather than the mean overtopping rate.

Several prediction methods exist to estimate $q$ (e.g. Molines and Medina, 2015a and EurOtop, 2018), the number of overtopping events ($N_{ow} = N_w\, P_{ow}$) and $V_{max}$ (see Molines et al., 2019) on mound

breakwaters in non-breaking conditions. Victor et al. (2012) conducted 2D physical tests on smooth impermeable structures under depth-limited breaking wave conditions with horizontal bottom slope and concluded that wave breaking had a significant impact on $N_{ow}$ and $V_{max}$. Gallach (2018) carried out 2D physical tests on smooth impermeable steep sloped structures in depth-limited breaking wave conditions and two bottom slopes ($m$ = 0 and $m$ = 1/100). However, Gallach (2018) did not find a significant effect of the breaking waves conditions on $V_{max}$. Nørgaard et al. (2014) performed 2D physical tests on rubble mound breakwaters (cot$\alpha$ = 1.5, where $cot\ \alpha$ is the armor slope) in depth-limited breaking wave conditions with horizontal bottom slope. They evaluated the performance of the existing formulations, valid for non-breaking wave conditions, for observations in breaking wave conditions and concluded that existing formulas were underpredicting $N_{ow}$ and overpredicting $V_{max}$. Therefore, the depth-limited breaking wave conditions of the incoming waves may be a significant factor to consider.

The bottom slope highly affects the type of wave breaking at the toe of the structure. Herrera et al. (2017) pointed out that bottom slope directly influences mound breakwater design; the optimum point where wave characteristics are estimated needs to be determined when in depth-limited breaking wave conditions. Mares-Nasarre et al. (2020) found a significant effect of bottom slope on the overtopping layer thickness ($h_c$) and the overtopping flow velocity ($u_c$). Mares-Nasarre et al. (2020) also determined that the optimum point to estimate wave characteristics to calculate $h_c$ and $u_c$ was located at a distance of 3 times the water depth from the toe of the structure. However, the influence of the bottom slope on $V_{max}$ has not yet been analyzed.

This research focuses on the distribution of individual wave overtopping volumes $F(V)$ in depth-limited breaking wave conditions for mound breakwaters and the influence of bottom slope on $V_{max}$. This paper is organized as follows. In section 2, the literature on individual wave overtopping volumes is examined. Neither the optimum point to estimate wave characteristics nor the effect of bottom slope on $N_{ow}$ and $V_{max}$ was assessed by the studies in the literature. Section 3 describes the experimental setup with two bottom slopes ($m$ = 1/25 and $m$ = 1/50) and the experimental data analysis. 2D small-scale tests on mound breakwaters in depth-limited breaking wave conditions ($0.20 \leq H_{m0}/h_s \leq 0.90$) and three armor layers (Cubipod®-1L, rock-2L and cube-2L) were conducted. Section 4 assesses existing estimators for $N_{ow}$ and $V_{max}$. None of the existing estimators for mound breakwaters satisfactory describes $N_{ow}$ for very low $q$. In section 5, the optimum point to estimate wave characteristics when calculating $N_{ow}$ is determined and a new $N_{ow}$ estimator is developed. In section 6, the 2-parameter Weibull distribution is considered to fit $F(V)$; the influence of bottom slope on the two-parameter Weibull distribution is also investigated. The quadratic utility function proposed by Molines et al. (2019) is used in this study to take into account the higher relevance of the largest individual wave overtopping volumes for practical applications. In section 7, the performance of the new $N_{ow}$ and $V_{max}$ estimators is validated using $q$ estimators given in the literature. Finally, in section 8, conclusions are drawn.

## 2. Literature review

### *2.1. Individual wave overtopping volumes*

Van der Meer and Janssen (1994) and Franco et al. (1994) first introduced the Weibull distribution to describe individual wave overtopping volumes for dikes, and vertical and composite breakwaters, respectively. Later, the 2-parameter Weibull distribution was proposed by different authors (e.g., Besley, 1999 or Victor et al., 2012) to analyze individual wave overtopping volumes in a variety of coastal structures. The 2-parameter Weibull distribution is given by

$$F(V) = F(x \leq V) = 1 - exp\left[-\left(\frac{V}{a}\right)^b\right] \quad (1)$$

where $F(x \leq V)$ is the non-exceedance probability of the individual wave overtopping volume per wave, $x$ is the individual wave overtopping volume, $a$ is the dimensional scale factor and $b$ is the shape factor. Eq. (1) can also be found as:

$$F(V) = 1 - exp\left[-\left(\frac{V/\bar{V}}{A}\right)^{b}\right] \quad (2)$$

where $A = a/\bar{V}$ is the scale factor and $\bar{V}$ is the measured mean individual wave overtopping volume.

If all the measured data were used for the analysis and they followed a perfect Weibull distribution, the mean individual wave overtopping volume, $\bar{V}$, would be equal to the mean value of the Weibull distribution, $\mu$ ($\mu = \bar{V}$). Under the previous hypothesis, a relationship between $A$ and $b$ exists and is described by

$$A = \frac{a}{\bar{V}} = \frac{1}{\Gamma\left(1+\frac{1}{b}\right)} \quad (3)$$

where $\Gamma$ is the gamma function, given by $\Gamma(z) = \int_0^\infty t^{z-1}\, e^{-t}\, dt$. Van der Meer and Janssen (1994) and Franco et al. (1994) recommended a value of $b$ = 0.75 for dikes, and vertical and composite breakwaters, respectively, which corresponds to $A$ = 0.84 according to Eq. (3).

Besley et al. (1999) studied individual wave overtopping volumes for sloped structures, vertical walls and composite breakwaters. These authors also referred to the results reported by Franco et al. (1996), who highlighted the influence of wave steepness on shape factor $b$ for vertical walls. Franco et al. (1996) also noticed that the shape factor $b$ was around 0.1 higher for sloping structures than for vertical walls. Regarding sloped structures, Besley et al. (1999) recommended values for the shape factor $b$ as a function of the offshore wave steepness, $s_{0p} = 2\pi H_{s0}/(gT_{p0}^2)$, where $H_{s0}$ is the significant offshore wave height and $T_{p0}$ is the deep water peak period. These authors suggested $b$ = 0.76 for $s_{op}$ = 0.02 and $b$ = 0.92 for $s_{op}$ = 0.04.

Bruce et al. (2009) carried out 2D physical tests on mound breakwaters with horizontal bottoms, $0.8 \le R_c/H_{m0} \le 1.3$ and $0.33 \le H_{m0}/h_s \le 0.40$, where $R_c$ is the crest freeboard, $H_{m0} = 4(m_0)^{1/2}$ is the significant wave height, and $h_s$ is the water depth at the toe of the structure. These authors tested a wide variety of armor units, both double- and single-layer armors, and analyzed the individual wave overtopping volumes higher than $\bar{V}$. Bruce et al. (2009) suggested a shape factor $b$ = 0.74 and concluded that no significant differences could be observed between the different armor units.

Victor et al. (2012) investigated individual wave overtopping volumes on smooth impermeable steep slopes ($0.36 \le cot\,\alpha \le 2.75$) with horizontal bottoms and $0.11 \le R_c/H_{m0} \le 1.69$. The authors observed that the wave heights during the tests with large $H_{m0}$ did not fit a Rayleigh distribution ($0.04 \le H_{m0}/h_s \le 0.37$), but a Composite Weibull distribution, and they concluded that deviations were caused by depth-induced breaking of the largest waves. Victor et al. (2012) also observed that this wave breaking process limited the value of the maximum individual wave overtopping volumes and decreased the shape factor $b$. Moreover, these authors investigated the effect of the relative crest freeboard, $R_c/H_{m0}$, slope angle, $\alpha$, and $s_{0p}$. They concluded that the effect of $s_{0p}$ ($0.012 \le s_{0p} \le 0.041$) was negligible and proposed Eq. (4) to estimate the shape factor $b$ considering the individual wave overtopping volumes higher than $\bar{V}$.

$$b = exp\left(-2.0\,\frac{R_c}{H_{m0}}\right) + (0.56 + 0.15\cot\alpha) \quad (4)$$

Zanuttigh et al. (2013) analyzed the shape factor $b$ for rough and smooth low-crested structures ($0 \le R_c/H_{m0} \le 2$), using the individual wave overtopping volumes higher than $\bar{V}$. These authors reported higher scatter in the data for rubble mound breakwaters than in the data for smooth slopes. Zanuttigh et al. (2013) also pointed out that, even if formulas considering the dimensionless crest freeboard ($R_c/H_{m0}$) gave good results for smooth structures, they were not adequate for rubble mound breakwaters. The shape factor $b$ for rubble mound breakwaters was found to be related to a dimensionless mean wave overtopping discharge, $Q^{**}=q/(g\,H_{m0}\,T_{m-1,0})$ (where $T_{m-1,0} = \frac{m_{-1}}{m_0}$ and $m_k$ is the $k$-$th$ spectral moment, $m_k = \int_0^\infty S(f) f^k df$, and $S(f)$ is the wave spectrum) similar to $Q^{*}=q/(g\,H_{m0}\,T_{01})$ (where $T_{01} = \frac{m_0}{m_1}$) proposed by Besley (1999), and Eq. (5) was derived. EurOtop (2018) also recommends Eq. (5) for estimating the shape factor $b$ for armored rubble slopes and mounds.

$$b = 0.85 + 1500\, Q^{**1.3} \quad (5)$$

Nørgaard et al. (2014) conducted 2D physical tests on rock-armored mound breakwaters with crown wall both in non-breaking and breaking wave conditions ($0.18 \leq H_{m0}/h_s \leq 0.50$) with horizontal bottoms and $0.9 \leq R_c/H_{m0} \leq 2.0$. These authors assessed the existing formulas in the literature for the shape factor $b$ in non-breaking wave conditions and concluded that they were overpredicting the largest overtopping wave volumes in depth-limited breaking wave conditions. Nørgaard et al. (2014) proposed Eq. (6) based on 30% of the highest individual wave overtopping volumes.

$$b = \begin{cases} 0.75 & for\ \frac{H_{m0}}{H_{1/10}} \leq 0.848\ or\ \frac{H_{m0}}{h_s} \leq 0.2 \\ -6.1 + 8.08\ \frac{H_{m0}}{H_{1/10}} & for\ \frac{H_{m0}}{H_{1/10}} > 0.848\ and\ \frac{H_{m0}}{h_s} > 0.2 \end{cases} \quad (6)$$

where $H_{1/10}$ is the average of 10% of the highest waves in the test run.

Gallach (2018) carried out thousands of 2D physical tests using bottom slopes $m$ = 0 and $m$ = 1/100 for steep slopes and vertical structures in a wide range of crest freeboards ($0.0 \leq R_c/H_{m0} \leq 3.25$). The author investigated the effect of depth-limited breaking wave conditions ($0.03 \leq H_{m0}/\ h_s \leq 0.50$) on the shape factor $b$ and found it negligible, contrary to results published by Victor et al. (2012) and Nørgaard et al. (2014). Gallach (2018) also noticed that the shape factor $b$ was not affected by the roughness of the structure and proposed a new formula to estimate $b$ as function of $R_c/H_{m0}$ and the structure slope, using the largest 10% individual wave overtopping volumes. Regarding the scale factor $A$, Gallach (2018) found that the best fit values were significantly different than those given by Eq. (3).

Molines et al. (2019) analyzed the 2D physical tests conducted by Smolka et al. (2009) on conventional mound breakwaters ($1.25 \leq R_c/H_{m0} \leq 4.78$) with crown wall in non-breaking conditions ($0.10 \leq H_{m0}/\ h_s \leq 0.32$) and reported the inconsistencies in the selection criteria of the number of overtopping events used to fit the scale and shape factors identified by Pan et al. (2016). Molines et al. (2019) compared the fitting of $A$ and $b$ of the 2-parameter Weibull distribution using 10%, 30% 50%, and 100% (with quadratic utility function) of the highest individual wave overtopping volumes. Utility functions are used to consider the relative relevance of the observed data; using the whole dataset with a quadratic utility function, all the observations are used but special attention is paid to the highest volumes. The relationship between $A$ and $b$ was not given any more by Eq. (3). Note that small overtopping events significantly affect $\bar{V}$ and $N_{ow}$; the estimations of $A$ based on Eq. (3) are sensitive to small overtopping events which are not significant for practical applications. The shape factor, $b$, is given as function of the dimensionless mean wave overtopping discharge, $Q^* = q/(g\ H_{m0}\ T_{01})$, whereas the scale factor $A$ depends on the shape factor $b$, as shown in Eqs. (7) and (8), respectively, when applying the quadratic utility function to all observed individual wave overtopping volumes.

$$b = 0.63 + 1.25 \exp\left(-3.0 \cdot 10^5\ Q^*\right) \quad (7)$$

$$A = 1.4 - 0.4\ \frac{1}{b} \quad (8)$$

Additionally, Molines et al. (2019) proposed a 2-parameter Exponential distribution to describe individual wave overtopping volumes, given by

$$F(V) = 1 - exp\left[-\left(\frac{V/\bar{V} - C}{D}\right)\right] \quad (9)$$

where

$$D = 2.6 - 2.6 \exp\left(-3.0 \cdot 10^5\ Q^*\right) \quad (10)$$

$$C = 1.2 - D - 0.2\ D^2 \quad (11)$$

### *2.2. Number of overtopping events*

In order to assign an exceedance probability to every individual wave overtopping volume, Makkonen (2006) recommended the Weibull plotting position formula, given by

$$F(V) = 1 - \frac{i}{N_{ow}+1} \tag{12}$$

where $F(V)$ is the exceedance probability of the individual wave overtopping volume per wave, $i$ is the rank of the individual volume, sorted in descending order ($i$ = 1 corresponds to $V_{max}$) and $N_{ow}$ is the number of overtopping events.

Lykke-Andersen et al. (2009) applied Eq. (12) to rewrite the Weibull distribution function as:

$$V_i = A\bar{V}\left[-\ln\left(\frac{i}{N_{ow}+1}\right)\right]^{1/b} = A\bar{V}\left[\ln(N_{ow}+1) - \ln(i)\right]^{1/b} \quad with\ i = 1\ to\ N_{ow} \tag{13}$$

By setting $i$ = 1 in Eq. (13), $V_{max}$ can be calculated as

$$V_{max} = A\bar{V}\left[\ln(N_{ow}+1)\right]^{1/b} \tag{14}$$

Besley (1999), EurOtop (2007) and EurOtop (2018) proposed Eq. (15), which uses $N_{ow}$ instead of $N_{ow} + 1$.

$$V_{max} = A\bar{V}\left[\ln(N_{ow})\right]^{1/b} \tag{15}$$

Lykke-Andersen et al. (2009) warned that Eq. (15) would predict an inconsistent $V_{max}$ = 0 for $N_{ow}$ = 1. To estimate $V_{max}$, not only $N_{ow}$ has to be estimated, using either Eq. (14) or Eq. (15), but also the mean individual wave overtopping volume ($\bar{V} = q\,T_{01}\,N_w/N_{ow}$, where $q$ is the mean overtopping discharge). Thus, $q$ has to be estimated in order to calculate $V_{max}$. To this end, Besley (1999) proposed Eqs. (16) and (17) for simple slopes, and complex slope structures with return walls or berms, respectively.

$$P_{ow} = \frac{N_{ow}}{N_w} = exp\left[-K_1\left(\frac{R_c}{T_{01}\sqrt{g\,H_{m0}}}\frac{1}{\gamma_f}\right)^2\right] \tag{16}$$

$$\begin{cases} P_{ow} = 55.4\,Q^{*0.634} & for\ 0 < Q^* < 8\cdot 10^{-4} \\ P_{ow} = 2.5\,Q^{*0.199} & for\ 8\cdot 10^{-4} < Q^* < 10^{-2} \\ P_{ow} = 1 & for\ Q^* > 10^{-2} \end{cases} \tag{17}$$

where $P_{ow}$ is the proportion of overtopping waves, $N_{ow}$ is the number of overtopping events and $N_w$ is the number of incoming waves, $\gamma_f$ is the roughness factor, $H_{m0}$ is the spectral significant wave height, $Q^* = q/(g\,H_{m0}\,T_{01})$ and $q$ are the dimensionless and dimensional mean overtopping discharges, respectively. Besley (1999) recommended $K_1$ = 37.8 for structure slope $cot\,\alpha$ = 2 and $K_1$ = 63.8 for $cot\,\alpha$ = 1. Besley (1999) proposed Eq. (18) to estimate $q$.

$$\frac{q}{g\,T_{01}\,H_{m0}} = K_2\,exp\left[-K_3\frac{R_c}{T_{01}\sqrt{g\,H_{m0}}}\frac{1}{\gamma_f}\right] \tag{18}$$

where $K_2$ and $K_3$ are experimental coefficients function of $\alpha$. For $cot\,\alpha$ = 1.5, $K_2 = 8.84\cdot 10^{-5}$ and $K_3$ = 19.9.

Nørgaard et al. (2014) proposed a variation of Eq. (19) to extend the application of this equation to depth-limited breaking wave conditions for $0.006 \le P_{ow} \le 0.120$ and $7.3\cdot 10^{-7} \le Q^* \le 6.2\cdot 10^{-5}$, given by

$$N_{ow} = C_1\,Eq.(17)$$

$$C_1 = \begin{cases} 1 & for\ H_{m0}/H_{1/10} \le 0.848\ or\ H_{m0}/h_s \le 0.2 \\ -6.65 + 9.02\,\dfrac{H_{m0}}{H_{\frac{1}{10}}} & for\ H_{m0}/H_{1/10} > 0.848\ and\ H_{m0}/h_s > 0.2 \end{cases} \tag{19}$$

Nørgaard et al. (2014) recommended using CLASH Neural Network (CLASH NN), described by Van Gent et al. (2007), for $q$ estimation.

EurOtop (2018) recommended Eq. (20) for mound breakwaters with permeable crest berms.

$$P_{ow} = exp\left[-\left(\sqrt{-\ln 0.02}\,\frac{R_c}{Ru_{2\%}}\right)^2\right] \tag{20}$$

where $Ru_{2\%}$ is the wave run-up height exceeded by 2% of the incoming waves, calculated as

$$\frac{Ru_{2\%}}{H_{m0}} = 1.65\,\gamma_f\,\gamma_\beta\,\gamma_b\,\xi_{-1,0} \tag{21a}$$

199 with a maximum value of

$$\frac{Ru_{2\%}}{H_{m0}} = \min\left(1.00\,\gamma_{fsurging}\,\gamma_\beta\left[4.00 - \frac{1.50}{\sqrt{\xi_{-1,0}}}\right], 2.0\right) \tag{21b}$$

200 where $\gamma_{fsurging} = \gamma_f + (Ir_{-1,0} - 1.8)(1-\gamma_f)/8.2$; $\gamma_\beta$, the oblique wave attack factor and $\xi_{-1,0} =$
201 $\tan\alpha/\sqrt{2\pi H_{m0}/(g\,T_{m-1,0}{}^2)}$.

202 EurOtop (2018) suggested Eq. (22) to estimate $q$.

$$\frac{q}{\sqrt{g\,H_{m0}{}^3}} = 0.09\exp\left(-1.5\,\frac{R_c}{H_{m0}\,\gamma_f\,\gamma_\beta}\right) \tag{22}$$

203

204 Molines et al. (2019) recently proposed to estimate the proportion of overtopping waves, $P_{ow}$,
205 valid for $0.001 \le P_{ow} \le 0.20$ and $7.0\cdot10^{-8} \le Q^* \le 6.4\cdot10^{-5}$, using

$$P_{ow} = 480\,Q^{*0.8} \tag{23}$$

206 Similar to Nørgaard et al. (2014), Molines et al. (2019) recommended using CLASH NN for
207 estimating $q$. Table 1 summarizes the experimental ranges of the methods found in the literature.

| Author | Structure | Crown wall | $R_c/H_{m0}$ [-] | $H_{m0}/h_s$ [-] | $m$ [-] | $\cot\alpha$ [-] |
|---|---|---|---|---|---|---|
| **Bruce et al. (2009)** | Mound breakwaters | Yes | 0.80 – 1.03 | 0.33 – 0.40 | 0 | 2 |
| **Victor et al. (2012)** | Smooth impermeable steep slopes | No | 0.11 – 1.69 | 0.04 – 0.37 | 0 | 0.36 – 2.75 |
| **Zanuttigh et al. (2013)** | Smooth slopes and rubble mound breakwaters | - | 0 – 2 | – | – | 2 – 4 |
| **Nørgaard et al. (2014)** | Rubble mound breakwaters | Yes | 0.9 – 2 | 0.18 – 0.50 | 0 | 1.5 |
| **Gallach (2018)** | Steep slopes and vertical structures | No | 0 – 3.25 | 0.03 – 0.50 | 0, 1/100 | 0 – 0.27, 1.5 – 2.75 |
| **Molines et al. (2019)** | Mound breakwaters | Yes | 1.25 – 4.78 | 0.10 – 0.32 | 0 | 1.5 |

208 Table 1. Summary of the experimental ranges of the methods to estimate $V_{max}$ in the literature.

209 Table 2 presents a summary of the methods in literature to estimate $V_{max}$ on mound breakwaters or
210 permeable slopes.

| Author | $q$ [m³/s/m] | $P_{ow}$ [-] | $b$ [-] | $A$ [-] | $V_{max}$ [l/m] |
|---|---|---|---|---|---|

| | | | | | |
|---|---|---|---|---|---|
| **Besley (1999)** | $g\,T_{01}\,H_{m0}\,K_2\,exp\left[-K_3\frac{R_c}{T_{01}\sqrt{g\,H_{m0}}}\frac{1}{\gamma}\right.$ | ***Simple slopes***: $exp\left[-K_1\left(\frac{R_c}{T_{01}\sqrt{g\,H_{m0}}}\frac{1}{\gamma_f}\right)^2\right]$ Complex slopes: $\begin{cases}55.4\,Q^{*0.634} & 0 < Q^* < 8\,10^{-}\\ 2.5\,Q^{*0.199} & 8\,10^{-4} < Q^* < 10^{-}\\ 1 & Q^* > 10^{-2}\end{cases}$ | 0.76 for $s_{op}$ = 0.02<br>0.92 for $s_{op}$ = 0.04 | $\frac{1}{\Gamma\left(1+\frac{1}{b}\right)}$ | $A\bar{V}[\ln(N_{ow})]^{1/b}$ |
| **EurOtop (2018)** | $0.09\exp\left(-1.5\,\frac{R_c}{H_{m0}\,\gamma_f\,\gamma_\beta}\right)\sqrt{g\,H_{m0}^{3}}$ | $exp\left[-\left(\sqrt{-\ln 0.02}\,\frac{R_c}{Ru_{2\%}}\right)^2\right]$ | $0.85 + 1500\,Q^{**1.3}$ | $\frac{1}{\Gamma\left(1+\frac{1}{b}\right)}$ | $A\bar{V}[\ln(N_{ow})]^{1/b}$ |
| **Nørgaard et al. (2014)** | CLASH NN | $C_1 \times (Besley, 1999; compl.sl.)$ Where: $C_1 = -6.65 + 9.02\,\frac{H_{m0}}{H_{\frac{1}{10}}}^{*,2}$ | $-6.1 + 8.08\,\frac{H_{m0}}{H_{1/10}}^{*,3}$ | $\frac{1}{\Gamma\left(1+\frac{1}{b}\right)}$ | $A\bar{V}[\ln(N_{ow}+1)]^{1/b}$ |
| **Molines et al. (2019)** | CLASH NN | $480\,Q^{*0.8}$ | $0.63 + 1.25\exp(-3\,10^5 Q^*)$ | $1.4 - 0.4\frac{1}{b}$ | $A\bar{V}[\ln(N_{ow}+1)]^{1/b}$ |

Notes:

*,1 $K_2$ and $K_3$ are empirical coefficients function of $\alpha$. Here, for cot($\alpha$)=1.5, $K_2$ = 8.84· $10^{-5}$ and $K_3$ = 19.9

*,2 for $\frac{H_{m0}}{H_{\frac{1}{10}}} > 0.848$ *and* $\frac{H_{m0}}{h_s} > 0.2$; elsewise $C_1$=1.

*,3 for $\frac{H_{m0}}{H_{\frac{1}{10}}} > 0.848$ *and* $\frac{H_{m0}}{h_s} > 0.2$; elsewise b=0.75.

Table 2. Summary of the methods in the literature to estimate $V_{max}$ for mound breakwaters or slopes structures.

### *3.1. Experimental setup*

2D physical tests were conducted in the wave flume (30.0 m × 1.2 m × 1.2 m) of the Laboratory of Ports and Coasts at the *Universitat Politècnica de València* (LPC-UPV), with two bottom slope configurations and a piston-type wave maker. The first configuration involved a continuous ramp of 4% slope ($m$ = 1/25) all along the flume. The second configuration was formed by two ramps: a 6.3 m-long $m$ = 1/25 bottom slope, and a 9.0 m-long $m$ = 1/50 bottom slope. Figure 1 shows the longitudinal cross-sections of the LPC-UPV wave flume for both configurations as well as the locations of the wave gauges.

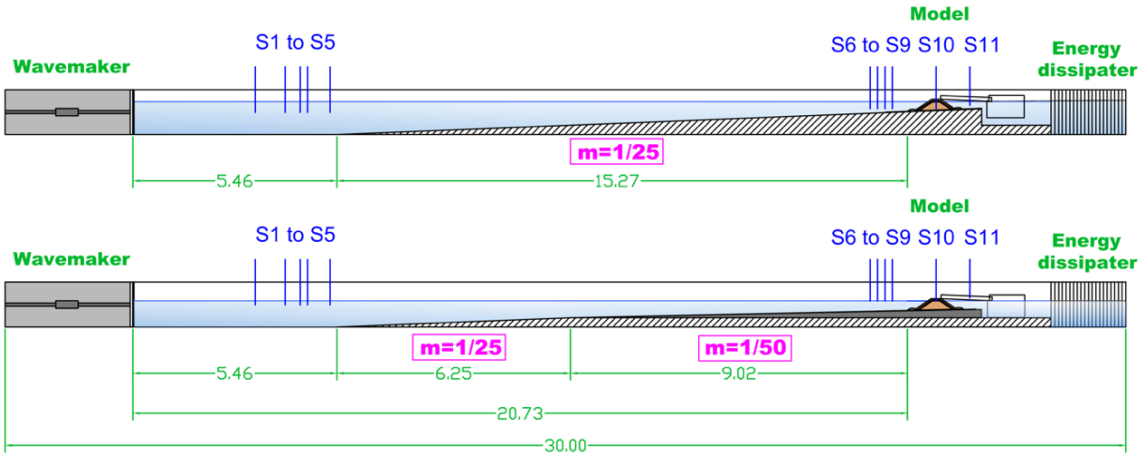


Figure 1. Longitudinal cross-section of the LPC-UPV wave flume (dimensions in meters).

In order to measure the water surface elevation, 11 capacitive wave gauges were placed along the flume. Wave gauges S1 to S5 were located in the wave generation zone, and these were used to

separate incident and reflected waves in the wave generation zone using the LASA-V method (see Figueres and Medina, 2004). Wave gauges S6 to S9 were placed close to the model, where depth-limited wave breaking occurs and existing methods to separate incident and reflected waves are not reliable. The distances from the structure toe to S6, S7, S8 and S9 were modified with the water depth at the toe of the structure, $h_s$. S6, S7, S8 and S9 were located at distances $5h_s$, $4h_s$, $3h_s$ and $2h_s$ from the toe of the breakwater, respectively, following the recommendations given by Herrera and Medina (2015). Wave gauge S10 was placed in the middle of the structure crest, and S11 was located behind the model.

Random wave runs of 1,000 waves were generated following a JONSWAP spectrum ($\gamma$=3.3). The AWACS wave absorption system was activated to avoid multireflections. Neither low-frequency oscillations nor piling-up (wave gauge S11) were significant during the tests. Piling-up consists of an increase of the water depth around the model caused by the accumulation of water when high overtopping rates occur. The LPC-UPV wave flume allows the water to be recirculated through a double floor of 25 cm to prevent it.

Test series were associated to the water depth at the toe of the model ($h_s$). For each $h_s$, $T_p$ and $H_{m0} = 4(m_0)^{0.5}$ at the wave generation zone were calculated so as to keep the wave steepness approximately constant throughout each test series ($s_{0p}$ = 0.018 and 0.049). For each $s_{0p}$, $H_{m0}$ at the wave generation zone ($H_{m0,g}$) was increased in steps of 1 cm from no damage to failure of the armor layer or wave breaking at the wave generation zone. The water depths at the toe of the structure were $h_s$ = 20 and 25 cm for the tests carried out with a bottom slope $m$ = 1/25. The water depths were $h_s$ = 20 and 25 cm for the single-layer Cubipod® and double-layer rock armored models with a bottom slope $m$ = 1/50. The water depths were $h_s$ = 25 and 30 cm for the double-layer cube armored model with a bottom slope $m$ = 1/50.

Due to the importance of crest freeboard on overtopping, two corrections were made: (1) the natural evaporation and facility leakages during the tests and (2) the extracted accumulated overtopping volumes during the working day (overtopping volumes in the collection tank were pumped out of the flume). These lead to a small increase in the crest freeboard along time of the order of 10 mm for a long working day.

The tested breakwater model corresponds to a mound breakwater with cot$\alpha$ = 1.5 slope and toe berms (see Figure 2). Three armor layers were tested: a single-layer Cubipod® armor, a double-layer rock armor and a double-layer randomly-placed cube armor. The nominal diameters or equivalent cube sizes were: $Dn$ = 3.79 cm (Cubipod®-1L), $Dn$ = 3.18 cm (rock-2L) and $Dn$ = 3.97 cm (cube-2L). Tests with the bottom slope $m$ = 1/50 were conducted with a medium size rock toe berm ($D_{n,50}$ = 2.6 cm), while tests with the bottom slope $m$ = 1/25 were carried out with a larger rock toe berm ($D_{n,50}$ = 3.9 cm) to guarantee the toe berm stability. The range of the variables in the test is shown in Table 3. Note that wave conditions in the model zone are estimated using the SwanOne model (see Verhagen et al., 2008), as explained in section 3.2.

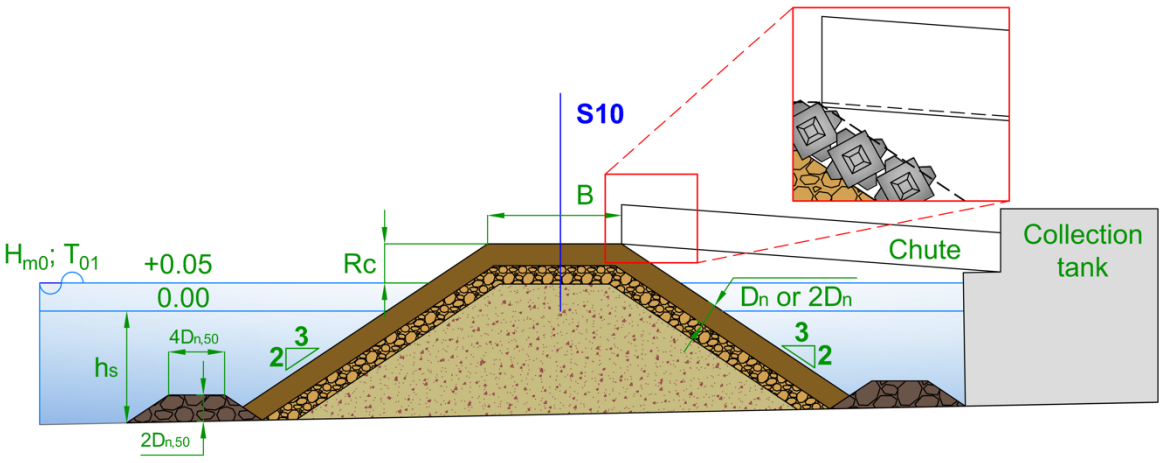


Figure 2. Cross-section of the breakwater model tested in LPC-UPV wave flume (dimensions in meters).

| $m$ | Armor | #tests | $B$ [m] | $h_s$ [m] | $R_c$ [m] | $H_{m0,g}$ [m] | $H_{m0}$ [m] | $T_{01}$ [s] |
|---|---|---|---|---|---|---|---|---|
| 1/50 | CC-1L | 47 | 0.24 | 0.20 | 0.12 | 0.06 – 0.21 | 0.06 – 0.15 | 0.83 – 1.97 |
| | | | | 0.25 | 0.07 | 0.06 – 0.21 | 0.06 – 0.16 | 0.87 – 2.02 |
| | CB-2L | 45 | 0.27 | 0.25 | 0.11 | 0.06 – 0.19 | 0.05 – 0.16 | 0.86 – 2.03 |
| | | | | 0.30 | 0.06 | 0.06 – 0.20 | 0.06 – 0.18 | 0.83 – 1.88 |
| | CE-2L | 13 | 0.26 | 0.20 | 0.15 | 0.06 – 0.13 | 0.06 – 0.12 | 0.81 – 1.66 |
| | | | | 0.25 | 0.10 | 0.06 – 0.13 | 0.06 – 0.13 | 0.82 – 1.71 |
| 1/25 | CC-1L | 46 | 0.24 | 0.20 | 0.12 | 0.07 – 0.21 | 0.06 – 0.15 | 0.84 – 1.65 |
| | | | | 0.25 | 0.07 | 0.07 – 0.21 | 0.06 – 0.18 | 0.82 – 2.11 |
| | CB-2L | 47 | 0.27 | 0.20 | 0.11 | 0.06 – 0.20 | 0.05 – 0.16 | 0.87 – 1.69 |
| | | | | 0.25 | 0.06 | 0.06 – 0.21 | 0.06 – 0.17 | 0.87 – 2.12 |
| | CE-2L | 21 | 0.26 | 0.20 | 0.15 | 0.06 – 0.16 | 0.05 – 0.14 | 0.84 – 1.86 |
| | | | | 0.25 | 0.10 | 0.06 – 0.13 | 0.05 – 0.14 | 0.80 – 1.88 |

Table 3. Dimensions and wave conditions at the toe of the structure in 2D physical tests at the LPC-UPV wave flume: CC-1L, CB-2L and CE-2L correspond to Cubipod® - 1L, cube-2L and rock-2L armors.

Overtopping discharges were measured using a weighing system placed in a collection tank behind the model during each test. Overtopping was collected using a chute in the rear side line of the crest. The inner border of the base of the chute was aligned with the armor layer to prevent too much wave overtopping losses. Individual wave overtopping volumes were identified following the method developed by Molines et al. (2019), based on a continuous record of accumulated overtopping volume. This method uses the derivative of the overtopping record to identify the overtopping volumes. Figure 3 shows a photo of the experimental set up with the Cubipod®-1L armored breakwater model.

Figure 3. Experimental set up with the Cubipod®-1L armored breakwater model.

### *3.2. Wave analysis*

Incident and reflected waves were separated in the wave generation zone using wave gauges S1 to S5 applying the LASA-V method (see Figueres and Medina, 2004). Although the LASA-V method is applicable to nonstationary and nonlinear irregular waves, it is not valid for breaking waves.

In order to estimate the incident wave conditions in the model zone, where wave breaking takes place, SwanOne software was used. This model assumes a Composite Weibull distribution to describe the wave height distribution in shallow foreshores, as suggested by Battjes and Groenendijk

(2000). Following the methodology proposed by Herrera and Medina (2015), the incident wave height in the depth-induced wave breaking zone was estimated with the SwanOne model using the incident waves at the wave generation zone. SwanOne model fits a JONSWAP spectrum ($\gamma$=3.3) based on the given incident wave conditions in the wave generation zone and propagates such fitted wave conditions along a given bathymetry. Herrera and Medina (2015) validated this method comparing the numerical SwanOne simulations with the measurements in the wave flume conducted without any structure. The results of the validation in this study are given in Figure 4 for both the wave generation zone (Figure 4 (a) and (c)) and the model zone (Figure 4 (b) and (d)).

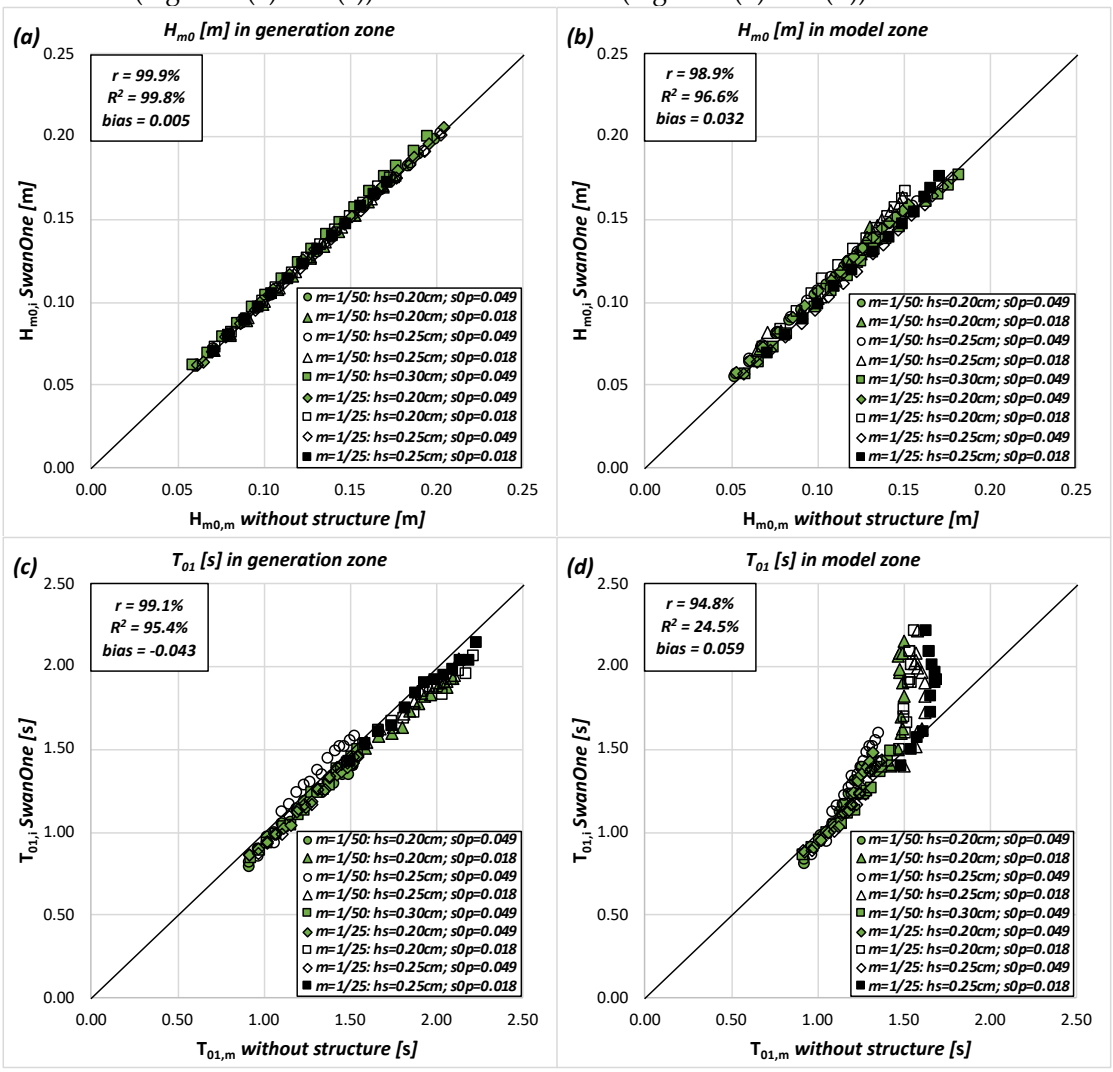


Figure 4. Comparison between: (a) the incident wave height obtained with the SwanOne and the measured significant wave height without a structure in generation zone, (b) the incident wave height obtained with the SwanOne and the measured significant wave height without a structure in model zone, (c) the incident mean period obtained with the SwanOne and the measured mean period without a structure in generation zone and (d) the incident mean period obtained with the SwanOne and the measured mean period without a structure in model zone.

To quantify the goodness of fit in this study, the correlation coefficient ($r$), the coefficient of determination ($R^2$) and the relative bias ($bias$) were calculated. $0 \leq r \leq 1$ assesses the correlation, $0 \leq R^2 \leq 1$ estimates the proportion of the variance explained by the model and $-1 \leq bias \leq 1$ provides a dimensionless measure of the bias. Thus, the higher the $r$, the higher the $R^2$ and the closer the $bias$ to 0, the better.

$$r = \frac{\sum_{i=1}^{N_o}(o_i - \bar{o})(e_i - \bar{e})}{\sqrt{\sum_{i=1}^{N_o}(o_i - \bar{o})^2 \sum_{i=1}^{N_o}(e_i - \bar{e})^2}} \quad (24)$$

$$R^2 = 1 - \frac{\frac{1}{N_o}\sum_{i=1}^{N_o}(o_i - e_i)^2}{\frac{1}{N_o}\sum_{i=1}^{N_o}(o_i - \bar{o})^2} \quad (25)$$

$$bias = \frac{1}{N_o}\sum_{i=1}^{N_o}\frac{(e_i - o_i)}{|o_i|} \quad (26)$$

where $N_o$ is the number of observations, $o_i$ and $e_i$ are the observed and estimated values, and $\bar{o}$ is the average observed value. Figure 4 shows that the agreement is very good for the fitted conditions in the wave generation zone ($R^2$ > 95.4%). On the other hand, in the model zone good agreement is obtained for $H_{m0}$ ($R^2$ = 96.6%) whereas poor results are observed for $T_{01}$ ($R^2$ = 24.5%). Note that decreasing values of *bias* were observed for $H_{m0}$ in the model zone for increasing values of $h_s$: *bias* = 0.057 for $h_s$ = 0.20cm, *bias* = 0.021 for $h_s$ = 0.25cm and *bias* = -0.018 for $h_s$ = 0.30cm. SwanOne clearly overestimates $T_{01}$ measured at the model area.

During the design phase of a mound breakwater, the design wave conditions ($H_{m0}$ and $T_{01}$) in the location where the structure will be built need to be estimated. Thus, in this study, both $H_{m0}$ and $T_{01}$ estimated by SwanOne were used.

## 4. Estimations of $N_{ow}$ and $V_{max}$ with methods given in the literature

In this section, the performance of the formulas to estimate $N_{ow}$ and $V_{max}$ presented in Section 2 is analyzed using the experimental data described in Section 3. As mentioned in Section 2.2, the formulas given in the literature for estimating $N_{ow}$ and $V_{max}$ require knowing the mean individual wave overtopping volume, $\bar{V} = q\, T_{01}\, N_w/N_{ow}$. Therefore, $q$ needs to be estimated using formulas in the literature when direct observations are not available. As shown in Table 2, estimators for $q$ are suggested by the different authors of the methods to estimate $N_{ow}$ and $V_{max}$ on mound breakwaters. The goodness of fit of such estimators of $q$ was assessed using the experimental data presented in Section 3. Figure 5 compares the observed and predicted $Q^*$ using the estimators in Table 2.

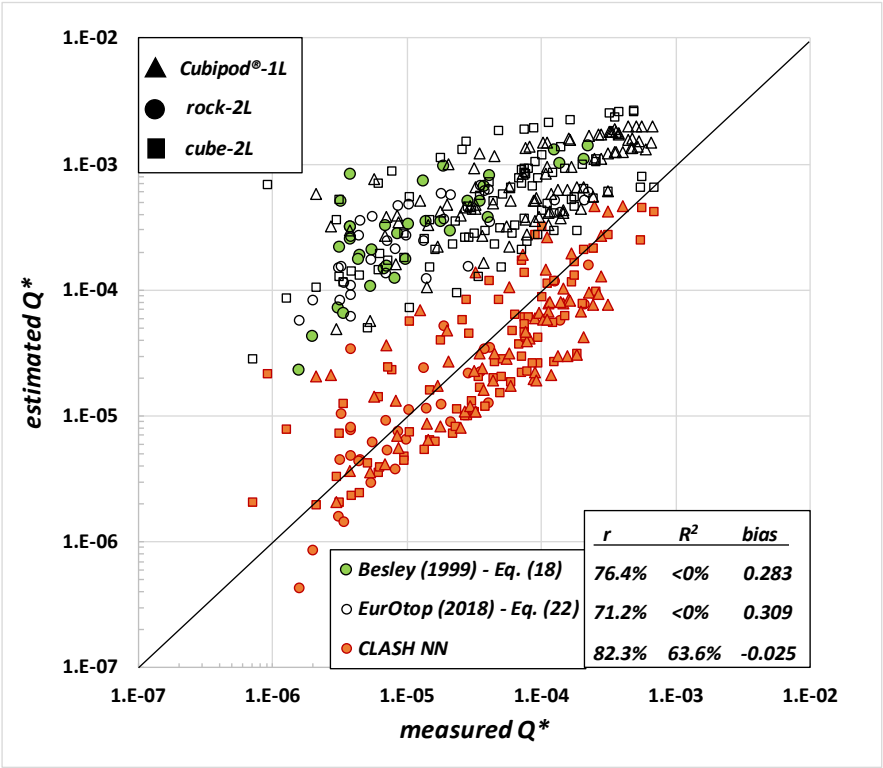


Figure 5. Comparison between measured and estimated $Q^*= q/(g\ H_{m0}\ T_{01})$.

The $q$ estimator recommended by Besley (1999) - Eq. (18) was applied using $\boldsymbol{\gamma_f}$ = 0.50 for rock-2L. Since this author did not propose $\boldsymbol{\gamma_f}$ for Cubipod®-1L and cube-2L, it was not applied on those data. The $q$ estimator proposed by EurOtop (2018) - Eq. (22) was used with $\gamma_f$ = 0.49, 0.40 and 0.47 for Cubipod®-1L, rock-2L and cube-2L, respectively. CLASH NN was applied with $\gamma_f$ recommemded by Molines and Medina (2015b): $\gamma_f$ = 0.48, 0.49 and 0.53 for Cubipod®-1L, rock-2L and cube-2L, respectively. $q$ was estimated for 189 physical tests within the range of application of CLASH NN.

Note that the quantitative goodness-of-fit metrics in Figure 5 are given for $ln(Q^*)$. As shown in Figure 5, poor results ($R^2$ < 0%) were obtained with the formulas given by Besley (1999) - Eq. (18) and EurOtop (2018) - Eq. (22). On the other hand, the predictor CLASH NN for $Q^*$ suggested by Molines et al. (2019) and Nørgaard et al. (2014) provided good results with $R^2$ = 63.6%.

### *4.1. Estimating $N_{ow}$ with existing methods*

In this section, the performance of the formulas to estimate $N_{ow}$ presented in Section 2.2 is assessed. Figure 6 compares the observed $N_{ow}$ with different estimators valid for mound breakwaters.

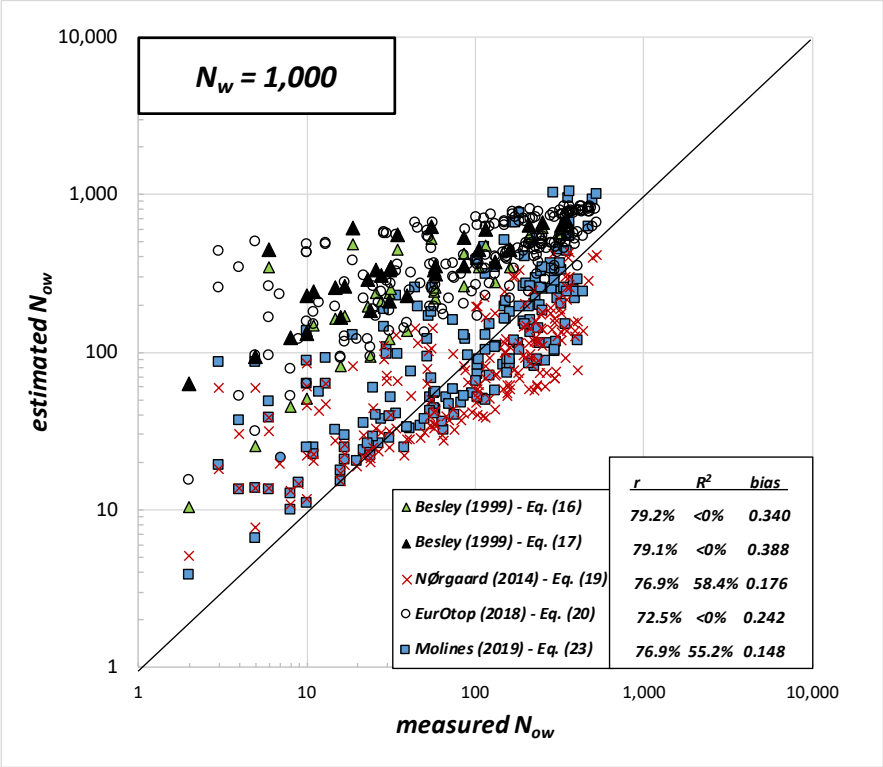


Figure 6. Comparison between measured and estimated $N_{ow}$ with methods given in the literature.

All formulas were applied no matter the application range. Note that estimated $q$ suggested by the authors of these formulas was used in the $N_{ow}$ predictors given by Besley (1999) - Eq. (17), Nørgaard et al. (2014) - Eq. (19) and Molines et al. (2019) - Eq. (23). The $N_{ow}$ estimator presented in Eq. (16) by Besley (1999) was applied using the roughness factor $\gamma_f$ = 0.50 for rock-2L. Since this author did not recommended $\gamma_f$ for Cubipod®-1L and cube-2L, it was not applied on those data. $K1$ = 50.8 was used with Eq. (16) for $cot\ \alpha$ = 1.5, obtained from the interpolation of the values given for $cot\ \alpha$ = 2 and $cot\ \alpha$ = 1. Eq. (20) was applied using $\gamma_f$ given by EurOtop (2018): $\gamma_f$ = 0.49, 0.40 and 0.47 for Cubipod®-1L, rock-2L and cube-2L, respectively.

The quantitative goodness-of-fit metrics are given for $ln(N_{ow})$. Eqs. (19) and (23) proposed by Nørgaard et al. (2014) and Molines et al. (2019), respectively, provided the best agreement with experimental data (55.2% < $R^2$ < 58.4%). Besley (1999) - Eqs. (16) and (17) and EurOtop (2018) – Eq. (20) overpredicted the values of $N_{ow}$ and provided poor results ($R^2$ < 0%). Note that all the compared methods from the literature overpredicted the values of $N_{ow}$ < 100. Figure 6 shows that that none of the existing $N_{ow}$ estimators properly describe $N_{ow}$ for the range of variables analyzed in this study. For this reason, a new $N_{ow}$ estimator is developed in Section 5.

### *4.2. Estimating $V_{max}$ with existing methods*

In Section 2, several formulas to estimate the shape factor $b$ were presented. Nevertheless, most of them are not valid for mound breakwaters. For this reason, only the formulas for mound breakwaters will be considered in the following comparison with the $V_{max}$ measured in this study.

In this analysis, $N_{ow}$ and $q$ are estimated with the methods proposed by the authors (see Table 2). The estimators for $N_{ow}$ and $q$ have been previously assessed in this Section. The scale factor, $A$, was calculated using Eq. (3) for Nørgaard et al. (2014) and EurOtop (2018), while Eq. (8) was applied for Molines et al. (2019). $V_{max}$ was estimated by Eq. (15).

Figure 7 compares the measured and the estimated dimensional $V_{max}$ (l/m) and the dimensionless $V_{max}^* = V_{max}/(g\ H_{m0}\ T_{01}^2)$ using the methods valid for mound breakwaters.

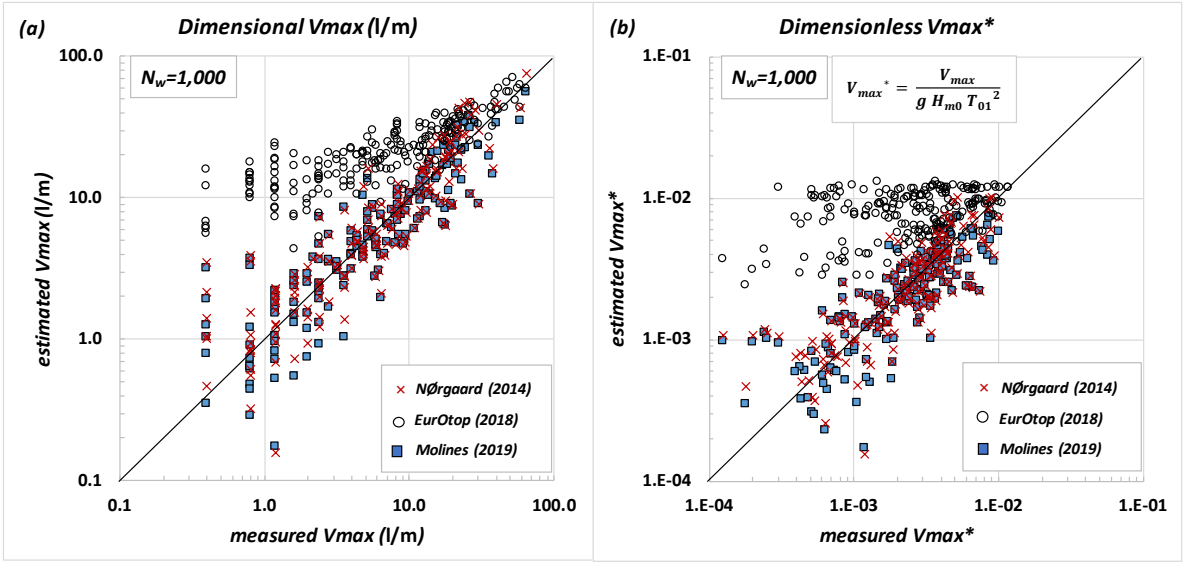


Figure 7. Comparison between measured and estimated (a) $V_{max}$ (l/m) and (b) dimensionless $V_{max}^*$.

$V_{max}^*$ measured in this study agreed well with estimations given by Nørgaard et al. (2014) and Molines et al. (2019) with higher scatter for $V_{max} < 5$ l/m and $V_{max}^* < 2 \cdot 10^{-3}$. Note that Molines et al. (2019) was developed for mound breakwaters with crown wall in non-breaking wave conditions. Thus, depth-limited breaking may not have a significant effect on $V_{max}^*$. Table 4 presents the quantitative measurements of the goodness of fit as well as the number of variables and parameters of the methods shown in Figure 7. The quantitative goodness-of-fit metrics in Table 4 are given for $ln(V_{max})$ and $ln(V_{max}^*)$.

| Author | | $V_{max}$ (l/m) | $V_{max}^*$ (-) | # parameters | # variables |
|---|---|---|---|---|---|
| Nørgaard et al. (2014) | $r$ | 88.8% | 79.0% | 13 | 3 |
| | $R^2$ | 78.4% | 61.8% | | |
| | *bias* | 0.148 | -0.002 | | |
| EurOtop (2018) | $r$ | 83.0% | 38.2% | 12 | 4 |
| | $R^2$ | < 0% | < 0% | | |
| | *bias* | 2.222 | 0.173 | | |
| Molines et al. (2019) | $r$ | 89.1% | 79.8% | 7 | 1 |
| | $R^2$ | 78.8% | 63.0% | | |
| | *bias* | -0.023 | -0.017 | | |

Table 4. Goodness-of-fit metrics for the methods in the literature to estimate $V_{max}$.

## 5. Estimating of the number of overtopping events, $N_{ow}$

### *5.1. A new formula to estimate $N_{ow}$*

As shown in Section 2, most of the existing estimators of $P_{ow} = N_{ow}/N_w$ are a function of a power of $Q^*$, as Eqs. (17), (19) and (23). Methods by Nørgaard et al. (2014) - Eq. (19) and Molines et al. (2019) - Eq. (23) provide good results within their range of application, but they do not properly estimate $P_{ow}$ for very low or very large $Q^*$. When $Q^*$ is very small, $P_{ow}$ should tend to 0, and when $Q^*$ is very large, $P_{ow}$ should tend to 1. Therefore, an exponential model may be better than a power law of $P_{ow}$, because it is good for very low and very high values of $Q^*$.

In this study, a clear correlation was found between $P_{ow}$ and $Q^*$, as previously observed by Besley (1999), Nørgaard et al. (2014) and Molines et al. (2019). Therefore, an exponential function of $Q^*$ was proposed and $G_1$ and $G_2$ in $P_{ow} = exp\,(-G_1/\,Q^{*G2})$ were calibrated based on the 219 tests maximizing $R^2$ of $lnN_{ow}$. The three armor layers tested in this study are not distinguished in the analysis (Bruce et al., 2009).

As exposed in Section 1, in depth-limited breaking wave conditions, the optimum point where wave characteristics are estimated is relevant for design and needs to be determined (Mares-Nasarre et al., 2020). Thus, $G_1$ and $G_2$ were calibrated considering wave characteristics at several distances from the structure toe in $Q^*= q/(g\ H_{m0}\ T_{01})$. $H_{m0}$ and $T_{01}$ were estimated with SwanOne at distances $x$ = 0, $h_s$, $2h_s$, $3h_s$, $4h_s$, $5h_s$ and $6h_s$ from the model toe. No significant differences were observed; $G_1$ = -0.1 and $G_2$= 0.3 were obtained for $H_{m0}$ and $T_{01}$ estimated between the model toe and at $6h_s$ from the model toe. In this study, wave characteristics estimated at a distance of $3h_s$ from the model toe are used, following Herrera et al. (2017) and Mares-Nasarre et al. (2020) recommendations. Note that this distance is approximately the same as $x$ = $5H_{m0}$, suggested by Melby (1999) and Goda (1985) to determine wave characteristics in breaking wave conditions.Figure 8 compares the experimental data and Eq. (27) with $R^2$ = 91.9%, as well as the 90% error band.

$$P_{ow} = \frac{N_{ow}}{N_w} = exp\left(\frac{-0.1}{Q^{*0.3}}\right) \tag{27}$$

where $P_{ow}$ = $N_{ow}$ / $N_w$ is the proportion of overtopping waves and $Q^*$ is the dimensionless wave overtopping discharge, $Q^*$ = $q/(g\ H_{m0}\ T_{01})$.

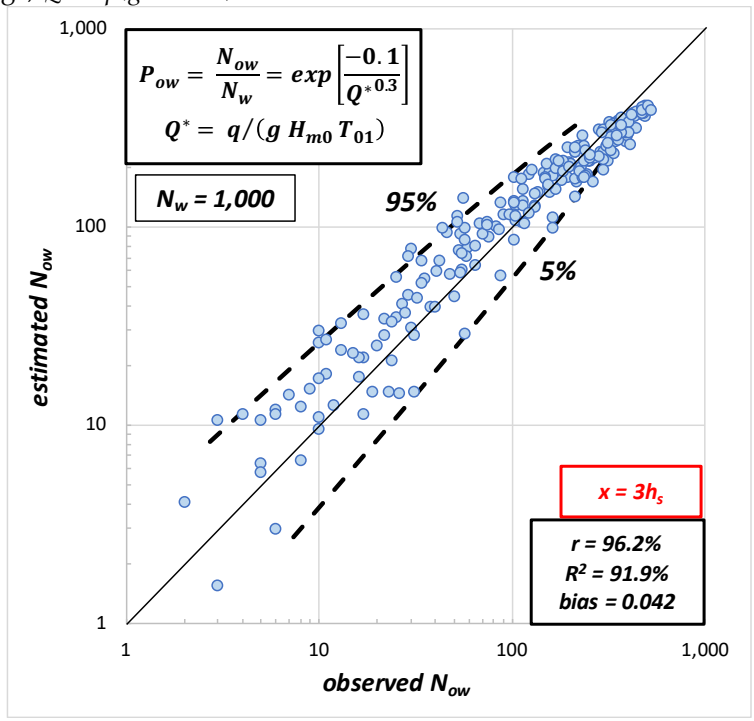


Figure 8. Comparison between observed number of overtopping events, $N_{ow}$, and estimated $N_{ow}$ given by Eq. (27) using wave characteristics estimated at a distance of $3h_s$ from the model.

In this study, the methodology given in Herrera and Medina (2015) and applied in works such as Mares-Nasarre et al. (2019) is used to estimate the 90% error band. Thus, a Gaussian distribution of the error (ε) is assumed, with 0 mean and the variance given by

$$\sigma^2(\varepsilon) = 0.55 - 0.09\ lnN_{ow} \tag{28}$$

The 95% and 5% percentiles for the $N_{ow}$ predicted by Eq. (27) can be calculated using Eq. (29).

$$lnN_{ow}|_{5\%}^{95\%} = lnN_{ow}\ \pm 1.64\sqrt{0.55 - 0.09\ lnN_{ow}} \tag{29}$$

The range of application of Eq. (26) is $0.002 \le P_{ow} \le 0.53$ and $7.2{\cdot}10^{-7} \le Q^* \le 6.9{\cdot}10^{-4}$. Eq. (26) properly extrapolates the prediction of $P_{ow}$=0 when $Q^*$=0 and $P_{ow}$=1 when $Q^*\rightarrow\infty$.

### *5.2. Influence of bottom slope on $N_{ow}$*

In Section 3, the experimental setup using two bottom slope configurations with $m$ = 1/50 and $m$ = 1/25 was described. No significant difference between bottom slopes $m$ = 1/50 and $m$ = 1/25 was observed in the scatter plot. A statistical analysis was performed to determine if $N_{ow}$ are equally distributed for different bottom slopes. Since the data were not Gaussian distributed, a nonparametric Mann-Whitney test (Mann and Whitney, 1947) was applied. In this test, the null hypothesis ($H_0$) corresponded to $N_{ow}$ not being affected by the bottom slope. Based on 103 tests with a bottom slope $m$ = 1/50 and 116 tests with a bottom slope $m$ = 1/25, $H_0$ was not rejected using a significance level $\alpha$ = 0.10. Thus, in this study the bottom slope does not show any significant influence on $N_{ow}$.

## 6. Estimating of the maximum individual wave overtopping volume, $V_{max}$

### *6.1. A new method to estimate $V_{max}$ using the 2-parameter Weibull distribution*

The maximum individual wave overtopping volume, $V_{max}$, is estimated using Eq. (15). Then, $V_{max}$ depends on the number of overtopping events, $N_{ow}$, shape and scale factors of the Weibull distribution, $A$ and $b$, and $\bar{V} = V_{total}/N_{ow}$. As previously mentioned, both $A$ and $b$ obtained for each test are fitted using a quadratic utility function applied to the whole individual wave overtopping volume dataset. Tests with very low values of $N_{ow}$ ($N_{ow}$ < 5) were not used in this analysis to prevent inconsistencies caused by a very low number of observations. Eqs. (30) and (31) were proposed to characterize $A$ and $b$

$$b = K_{B1} + \exp(K_{B2}\, Q^*) \tag{30}$$

$$A = 1.45 - 0.4/b \tag{31}$$

Similar to Section 5.1, $K_{B1}$ and $K_{B2}$ were calibrated considering wave characteristics at several distances from the structure toe in $Q^*= q/(g\, H_{m0}\, T_{01})$. $H_{m0}$ and $T_{01}$ were determined with SwanOne at distances $x$ = 0, $h_s$, 2$h_s$, 3$h_s$, 4$h_s$, 5$h_s$ and 6$h_s$ from the structure toe. The goodness-of-fit of $V_{max}^* = V_{max}/(g\, H_{m0}\, T_{01}^2)$ was assessed for every couple of coefficients calculated using Eqs. (15), (30) and (31) with the measured $N_{ow}$ and $\bar{V}$. Best fit was obtained between $x$ = 2$h_s$ and $x$ = 6$h_s$, $K_{B1}$ = 0.8 and $K_{B2}$ = = -2·10$^5$ were obtained with $r$ = 92% and $R^2$ = 83%. Wave characteristics were decided to be estimated at $x$ = 3$h_s$.

Figure 9a illustrates the relationship between $Q^*$ and $b$ and the least-squares fitting given by Eq. (30). Figure 9b relates $A$ and $1/b$ and the least-squares fitting given by Eq. (31). The range of application of Eqs. (30) and (31) is 0.005 ≤ $P_{ow}$ ≤ 0.53 and 1.3·10$^{-6}$ ≤ $Q^*$ ≤ 6.9·10$^{-4}$.

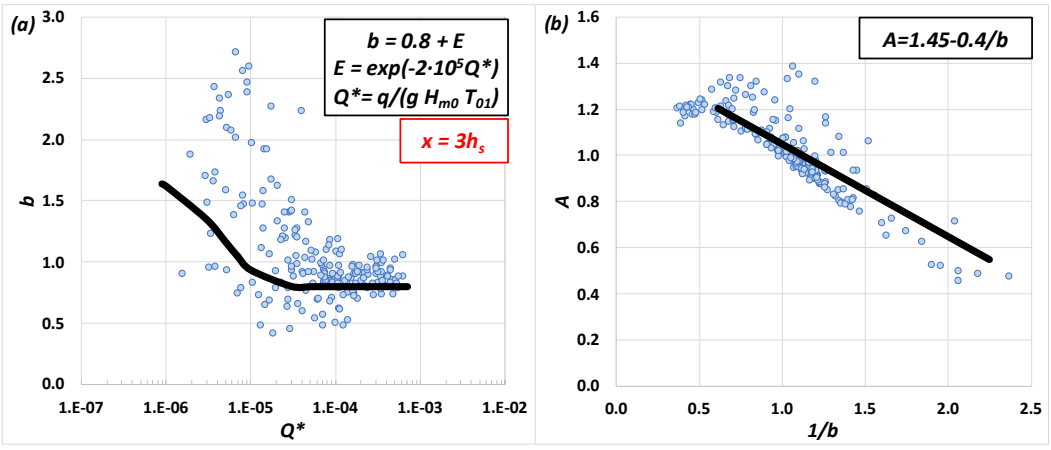


Figure 9. Relationship between explanatory variables and the least-squares fitting of Weibull distribution factors: (a) Weibull's shape factor, $b$, in Eq. (30) and (b) Weibull's scale factor, $A$, in Eq. (31).

Figure 10 illustrates the performance of Eq. (15) to estimate $V_{max}^* = V_{max}/(g\, H_{m0}\, T_{01}^2)$ when using $A$ and $b$ obtained from Eqs. (30) and (31) and measured $N_{ow}$ and $\bar{V}$. The agreement was good; $R^2$ = 83.3%.

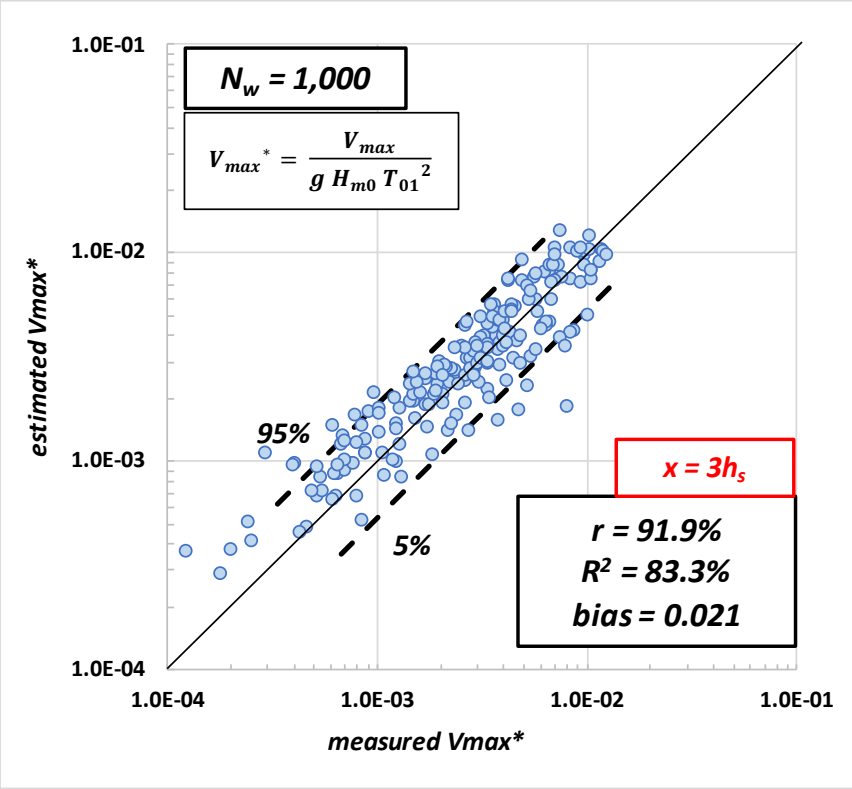


Figure 10. Comparison between the measured and estimated dimensionless $V_{max}^*$ by the 2-parameter Weibull distribution with shape and scale factors given by Eqs. (30) and (31).

The variance of the error (ε) of $lnV_{max}^*$ is $\sigma^2(\varepsilon) = 0.15$. Thus, the 95% and 5% percentiles for the predicted $V_{max}^*$ by Eq. (15) are given by

$$lnV_{max}^*|_{5\%}^{95\%} = lnV_{max}^* \pm 0.63 \tag{32}$$

Figure 11 shows an example of the fit of the 2-parameter Weibull distribution to the measured individual wave overtopping volumes for a randomly-selected test (#22). Figure 11 is presented in a Weibull plot:

$$\ln\left(-\ln\left(1 - F(V)\right)\right) = b(\ln\,(V/\bar{V}) - \ln\,(A)) \tag{33}$$

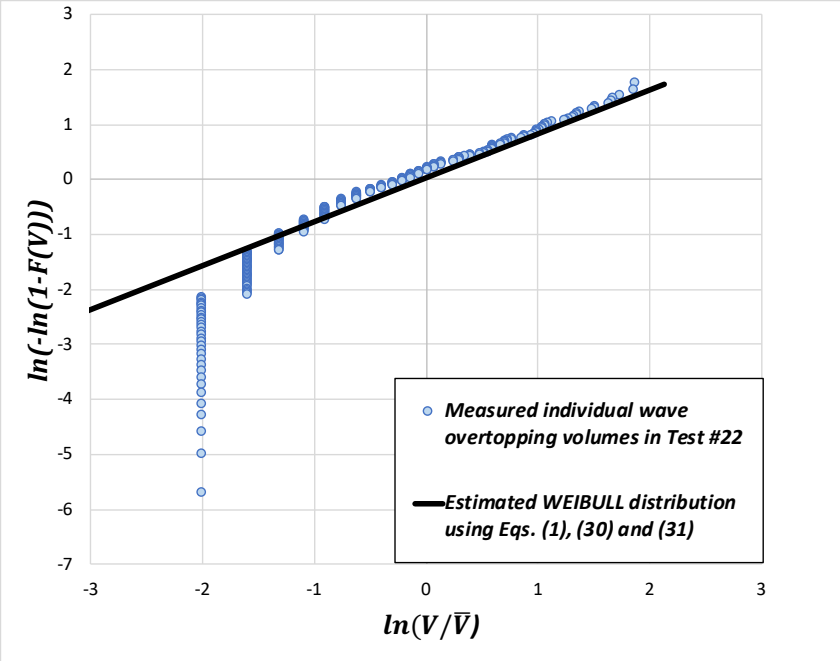


Figure 11. Comparison of measured and estimated individual wave overtopping volumes for Test #22 using Eqs. (1), (30) and (31).

As explained in Section 2, Molines et al. (2019) proposed a 2-parameter Exponential distribution given by Eq. (9) to describe $F(V)$. In this study, the 2-parameter Exponential distribution was also fitted with good results.

### *6.2. Influence of bottom slope on the 2-parameter Weibull distribution*

As presented in section 5.2, the influence of bottom slope on $b$ and $A$ estimated by Eqs. (30) and (31) is studied here. No relevant differences between the bottom slopes $m$ = 1/50 and $m$ = 1/25 were found. The Mann-Whitney test was applied for each parameter, as described in section 5.2. The null hypothesis ($H_0$) corresponded to $b$ and $A$ not being influenced by the bottom slope. Based on 97 tests with a bottom slope $m$ = 1/50 and 106 tests with a bottom slope $m$ = 1/25, $H_0$ was not rejected using a significance level $\alpha$ = 0.10. Thus, in this case bottom slope does not show any significantly influence on $V_{max}$.

## 7. Estimation of $V_{max}$ for mound breakwater designs

During the design phase of a mound breakwater, the design wave conditions ($H_{m0}$ and $T_{01}$) and the structural geometry are given. The formulas given in the literature require knowing the mean individual wave overtopping volume, $\bar{V} = q\ T_{01}\ N_w/N_{ow}$, and the number of overtopping events, $N_{ow}$. Therefore, $q$ and $N_{ow}$ need to be estimated using formulas in the literature when direct observations (e.g. sections 5 and 6) are not available. Methods suggested in the literature to estimate $q$ were assessed in Section 4. The best fit was given by CLASH NN with $R^2$ = 63.6%. Thus, $Q^*$ estimated with CLASH NN was used in the following. When using Eq. (27) developed in this study to calculate $N_{ow}$ estimating $q$ with CLASH NN, $r$ = 77.1%, $R^2$ = 58.4% and *bias* = 0.026. The agreement was worse than $R^2$ = 91.9% (see Figure 8) obtained when $q$ is measured and not estimated. Note that the fitting of the new formula is equal to the one obtained with the method proposed by Nørgaard et al. (2014) (see Figure 6). However, the method proposed by Nørgaard et al. (2014) to estimate $N_{ow}$ requires 3 variables and 10 parameters, while the method developed in this study uses 1 variable and 2 parameters.

Figure 12 illustrates the goodness of fit of Eq. (15) to estimate $V_{max}$ based on the estimations of $N_{ow}$ and $\bar{V}$ when $q$ is estimated using CLASH NN. Eqs. (30) and (31) were applied to estimate the

Weibull parameters ($A$, $b$). $R^2$ = 61.7% was obtained for $V_{max}^* = V_{max}/(g\,H_{m0}\,T_{01}^2)$. Figure 12 also presents the estimations given by Nørgaard et al. (2014) and Molines et al. (2019) as well as the 90% error band.

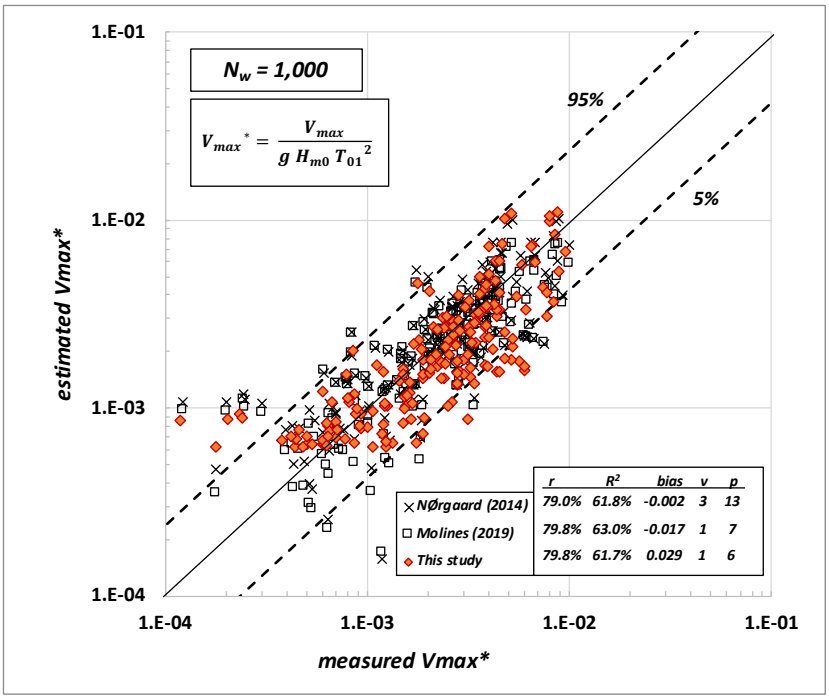


Figure 12. Comparison of measured dimensionless maximum individual wave overtopping volume, $V_{max}^*$, and the estimated $V_{max}$* for the Weibull distribution model using Eqs. (15), (30) and (31) and the methods for mound breakwaters in the literature.

As shown in Figure 12, the goodness of fit of the three compared methods is similar. However, the method proposed in the present study (1 variable ($v$) and 6 parameters ($p$)) is much simpler than the method proposed by Nørgaard et al. (2014) ($v$ = 3 and $p$ = 13) and simpler than the method proposed by Molines et al. (2019) ($v$ = 1 and $p$ = 7). Using the method proposed in this study, the ratio between estimated and measured $V_{max}^*$ for design purposes falls within a factor of 2.0 (90% error band).

## 8. Conclusions

Crest elevation of mound breakwaters is usually designed to limit the mean wave overtopping rate ($q$) or the maximum individual wave overtopping volume ($V_{max}$). Furthermore, rising sea levels caused by climate change and mounting social pressure to minimize the visual impact of coastal structures mean lower crest freeboards and increased overtopping hazards. Thus, coastal structure designs with relevant overtopping rates attacked by waves breaking on the sea bottom become relevant. Few studies have been conducted in depth-limited breaking wave conditions. This research is focused on mound breakwaters with significant overtopping rates ($0.002 \le P_{ow} \le 0.53$ and $7.2{\cdot}10^{-7} \le Q^*=q/(g\,H_{m0}\,T_{01}) \le 6.9{\cdot}10^{-4}$) and intermediate crest elevations ($0.33 \le R_c/H_{m0} \le 2.83$) with armor slope cot$\alpha$ = 1.5 in depth-limited breaking wave conditions ($0.2 \le H_{m0}/h_s \le 0.9$), considering two bottom slopes ($m$ = 1/50 and $m$ = 1/25).

In this study, 105 physical tests with a bottom slope $m$ = 1/50 and 114 tests with $m$ = 1/25 were conducted at the LPC-UPV wave flume. Individual wave overtopping volumes were analyzed using Molines et al. (2019) methodology, based on a continuous record of accumulated overtopping volume. In order to estimate the incident wave conditions in the model zone, where breaking occurs, SwanOne model was used. The performance of SwanOne when estimating wave characteristics under depth-limited breaking wave conditions was assessed using tests without structure. The agreement was good for $H_{m0}$ ($R^2$=96.6%), but some bias was observed for the shallowest water depth (*bias* = 0.057). The agreement was poor for $T_{01}$ ($R^2$=23.3%); SwanOne overestimated the measured $T_{01}$ in the model zone.

Estimators for $P_{ow}$ given in the literature were assessed using the experimental data; it was observed that most existing formulas overpredict $P_{ow}$ for $P_{ow} < 10\%$. Most of the existing $P_{ow}$ estimators are a function of a power of $Q^*$, so they cannot fit the boundary limits ($P_{ow} \to 0$ when $Q^* \to 0$ and $P_{ow} \to 1$ when $Q^* \to \infty$). Hence, a new exponential estimator is given for $P_{ow}$ valid for depth-limited breaking wave conditions in Eq. (27) ($R^2 = 91.9\%$).

The quadratic utility function proposed by Molines et al. (2019) was applied in this study to all the data to fit the 2-parameter Weibull distribution for individual wave overtopping volumes, $F(V)$. Estimators were taken from Nørgaard et al. (2014), EurOtop (2018) and Molines et al. (2019) for the scale ($A$) and shape ($b$) factors of the Weibull distribution to compare with the measured data, obtaining $0\% \leq R^2 \leq 63.0\%$ for the dimensionless maximum individual wave overtopping volume, $V_{max}^* = V_{max}/(g\, H_{m0}\, T_{01}^2)$. Best results using methods given in the literature were obtained for Molines et al. (2019) whose method was developed for mound breakwaters with crown wall in non-breaking wave conditions. Thus, the influence of the depth-induced wave breaking or the presence of the crest wall may not be significant.

New estimators for the factors $A$ and $b$ of the Weibull distribution were fitted using the experimental data. The new Weibull (Eqs. (30) and (31)) distribution provide estimations of $V_{max}^*$ with $R^2 = 83.3\%$ and a number of variables and parameters lower than those of the methods in the literature. In this study, no significant influence of bottom slope ($1/50 \leq m \leq 1/25$) was found on $N_{ow}$ and $V_{max}$.

During the design phase of a mound breakwater, the mean individual wave overtopping volume ($\bar{V} = q\, T_{01}\, N_w/N_{ow}$) is required to estimate $V_{max}$. But $q$ and $N_{ow}$ are unknown, and they have to be estimated using methods in the literature when direct observations are not available. Here, CLASH Neural Network (CLASH NN) was used to estimate $q$ with $R^2 = 63.6\%$. Using $q$ estimated by the CLASH NN and the new $N_{ow}$ estimator given in Eq. (27), $V_{max}^*$ was estimated with the 2-parameter Weibull distribution proposed in this study. The prediction error of $V_{max}^*$ dropped from $R^2 = 83.3\%$ when $q$ and $N_{ow}$ were measured in the laboratory to $R^2 = 61.7\%$ when $q$ was estimated with CLASH NN. The ratio between estimated and measured $V_{max}^*$ falls within a factor of 2.0 (90% error band) for design purposes.

The estimators and conclusions derived here are valid within the experimental ranges of this study. Therefore, it is encouraged to check their validity out of these experimental ranges, paying special attention to the significance of the depth-limited breakage of waves and the presence of a crown wall.

## Acknowledgements

The authors acknowledge the financial support from the *Ministerio de Economía y Competitividad* and *Fondo Europeo de Desarrollo Regional* (FEDER) under grant RTI2018-101073-B-I00, *Universitat Politècnica de València* (Grant SP20180111), *Primeros Proyectos de Investigación* (PAID-06-18), *Vicerrectorado de Investigación, Innovación y Transferencia de la Universitat Politècnica de València* and *Generalitat Valenciana* (Grant AEST/2019/004). The first author was also financially supported through the FPU program (*Formación de Profesorado Universitario*) funded by *Ministerio de Educación, Cultura y Deporte* under grant FPU16/05081. The authors thank Debra Westall for revising the manuscript.

## References

Battjes, J.A., Groenendijk, H.W., 2000. Wave height distributions on shallow foreshores, *Coastal Engineering* 40, 161-182. https://doi.org/10.1016/S0378-3839(00)00007-7

Besley, P., 1999. Overtopping of Sea-Walls-Design and Assessment Manual. R & D Technical Report, vol. 178 Environment Agency, Bristol, UK.

Bruce, T., van der Meer, J.W., Franco, L., Pearson, J.M., 2009. Overtopping performance of different armour units for rubble mound breakwaters. *Coastal Engineering* 56, 166–179. https://doi.org/10.1016/j.coastaleng.2008.03.015

EurOtop, 2007. *Wave Overtopping of Sea Defences and Related Structures: Assessment Manual (EurOtop Manual).* Environment Agency, UK/ENW Expertise Netwerk Waterkeren, NL/KFKI Kuratorium fuïr Forschung im Kuïsteningenieurwesen, Germany, pp. 193; Pullen, T., Allsop, N.W.H., Bruce, T., Kortenhaus, A., Schuïttrumpf, H., Van der Meer, J.W.

EurOtop, 2018. *Manual on wave overtopping of sea defences and related structures*. An overtopping manual largely based on European research, but for worldwide application. Van der Meer, J.W., Allsop, N.W.H., Bruce, T., De Rouck, J., Kortenhaus, A., Pullen, T., Schüttrumpf, H., Troch, P., Zanuttigh, B., www.overtopping-manual.com.

Figueres, M., Medina, J.R., 2004. Estimating incident and reflected waves using a fully nonlinear wave model, *Proc. 29th International Conference on Coastal Engineering*, World Scientific, 594-603. https://doi.org/10.1142/9789812701916-0047

Franco, L., de Gerloni, M., van der Meer, J.W., 1994. Wave overtopping on vertical and composite breakwaters. *Proc. 24th International Conference on Coastal Engineering*, ASCE, 1030-1044.

Gallach, D., 2018. Experimental Study of Wave Overtopping Performance of Steep Low-Crested Structures. PhD Thesis. Ghent University.

Goda, Y., 1985. *Random Seas and Design of Maritime Structures*; University of Tokyo Press: Tokyo, Japan.

Herrera, M.P., Medina, J.R., 2015. Toe berm design for very shallow waters, *Coastal Engineering* 103, 67-77. https://doi.org/10.1016/j.coastaleng.2015.06.005

Herrera, M.P.; Gómez-Martín, M.E.; Medina, J.R., 2017. Hydraulic stability of rock armors in breaking wave conditions. *Coastal Engineering* 127, 55–67. https://doi.org/10.1016/j.coastaleng.2017.06.010.

Lykke-Andersen, T., Burcharth, H.F., Gironella, F.X., 2009. Single wave overtopping volumes and their travel distance for rubble mound breakwaters. *Proc. 5th International Conference Coastal Structures 2007*, World Scientific, 1241–1252. https://doi.org/10.1142/9789814282024_0109

Makkonen, L., 2006. Plotting positions in extreme values analysis. *Journal of Applied Meteorology and climatology*, 45, 334–340. https://doi.org/10.1175/JAM2349.1

Mann, H.B., Whitney, D.R., 1947. On a test of whether one of two random variables is stochastically larger than the other. *The Annals of Mathematical Statistics* 18, 50-60 (5.3).

Mares-Nasarre, P., Gómez-Martín, M.E., Medina, J.R., 2020. Influence of Mild Bottom Slopes on the Overtopping Flow over Mound Breakwaters under Depth-Limited Breaking Wave Conditions. *Journal of Marine Science and Engineering* 8(1), 3. https://doi.org/10.3390/jmse8010003

Mares-Nasarre, P., Argente, G., Gómez-Martín, M.E., Medina, J.R., 2019. Overtopping layer thickness and overtopping flow velocity on mound breakwaters. *Coastal Engineering* 154, 103561. https://doi.org/10.1016/j.coastaleng.2019.103561

Melby, J.A., 1999. Damage Progression on Rubble Mound Breakwaters; Technical Report CHL-99-17; U.S. Army Engineer Research and Development Center: Vicksburg, MS, USA. Also Ph.D. Thesis, University of Delaware, Newark, DE, USA.

Molines, J., Medina, J.R., 2015a. Explicit wave overtopping formula for mound breakwaters with crown walls using CLASH neural network derived-data. *Journal of Waterway, Port, Coastal and Ocean Engineering*. 142 (3), 04015024. https://doi.org/10.1061/(ASCE)WW.1943-5460.0000322.

Molines, J., Medina, J.R., 2015b. Calibration of overtopping roughness factors for concrete armor units in non-breaking conditions using the CLASH database. *Coastal Engineering* 96, 65–70. https://doi.org/10.1016/j.coastaleng.2014.11.008

Molines, J., Herrera, M.P., Gómez-Martín, M.E., Medina, J.R., 2019. Distribution of individual wave overtopping volumes on mound breakwaters, *Coastal Engineering* 149, 15-27. https://doi.org/10.1016/j.coastaleng.2019.03.006

Nørgaard, J.Q.H., Lykke-Andersen, T., Burcharth, H.F., 2014. Distribution of individual wave overtopping volumes in shallow water wave conditions. *Coastal Engineering* 83, 15–23. https://doi.org/10.1016/j.coastaleng.2013.09.003

Pan, Y., Lin, L., Amini, F., Kuang, C., Chen, Y., 2016. New understanding on the distribution of individual wave overtopping volumes over a levee under negative freeboard. *Journal of Coastal Research,* 75, 1207–1211. https://doi.org/10.2112/SI75-242.1

Smolka, E., Zarranz, G., Medina, J.R., 2009. Estudio Experimental del Rebase de un Dique en Talud de Cubípodos. *Libro de las X Jornadas Españolas de Costas y Puertos*. Universidad de Cantabria-Adif Congresos, 803–809 (in Spanish).

Van der Meer, J.W., Janssen, J.P.F.M., 1994. Wave Run-Up and Wave Overtopping at Dikes, Delft Hydraulics No. 485, 22.

Van Gent, M.R.A., Van den Boogaard, H.F.P., Pozueta, B., Medina, J.R., 2007. Neural network modelling of wave overtopping at coastal structures. *Coastal Engineering* 54 (8), 586–593. https://doi.org/10.1016/j.coastaleng.2006.12.001.
Available: https://www.deltares.nl/en/software/overtopping-neural-network/, Accessed: 26 June 2019.

Verhagen, H.J., Van Vledder, G., Eslami Arab, S., 2008. A practical method for design of coastal structures in shallow water, *Proc. 31st International Conference on Coastal Engineering*, World Scientific, 2912-2922. https://doi.org/10.1142/9789814277426_0241

Victor, L., van der Meer, J.W., Troch, P., 2012. Probability distribution of individual wave overtopping volumes for smooth impermeable steep slopes with low crest freeboards. *Coastal Engineering* 64, 87–101. https://doi.org/10.1016/j.coastaleng.2012.01.003

Zanuttigh, B., van der Meer, J.W., Bruce, T., Hughes, S., 2013. Statistical characterization of extreme overtopping wave volumes. *Proc. Coasts, Marine Structures and Breakwaters*. 2014. ICE Publishing, (London, UK), 1, 442–452. https://doi.org/10.1680/fsts.59757.0442